OBSERVATIONS AND ANALYSIS OF STRUCTURES IN EXHUMED MINE-INDUCED FAULTS

A. McGarr and D. Pollard
U.S. Geological Survey
345 Middlefield Road
Menlo Park, CA 94025

N. C. Gay
Mining Operations Laboratory
Chamber of Mines of South Africa
Johannesburg, South Africa

W. D. Ortlepp
Rand Mines, Ltd.
Corner House
Johannesburg, South Africa

INTRODUCTION

It is well known that natural earthquake faults usually have considerable structural complexity and that a simple planar model of a fault is not entirely adequate. Faults induced by mining excavations (stopes) in deep gold mines show a similar degree of complexity and there are many advantages to studying them. They often occur in previously intact rock with known mechanical properties and much more is known about the state of stress in the hypocentral region than for natural faults. In many cases the rock in deep gold mines is dry so that studies of fault mechanics are not hindered by the uncertainties of possible hydraulic effects (e.g. McGarr et al., 1975). The best-studied mine-induced shear zones have formed in solid intact rock and then are later exhumed when the mine developnent finally penetrates into them. Thus, the mine excavations, at depths extending to below 3 km provide very direct evidence about the nature of faulting in the environs of the earthquake focus.

This report reviews observations of the structure of a mine-induced fault zone in the E.R.P.M. gold mine, east of Johannesburg, South Africa, and then relates consistent features of the shear zone complexity to theoretical fracture patterns based on the mechanics of shear crack formation and interactions between cracks. Finally, we draw conclusions regarding constraints on models for the developnent of the fault zones based on the underground observations in conjunction with results of laboratory testing.

The observations reviewed here were made from a network of tunnels developed into a fault system at a depth of 2 km in the West Claims pillar of ERPM (Ortlepp, 1978; Ortlepp and Gay, 1979; McGarr et al., 1979, Spottiswoode, 1979). This fracture system is undoubtedly the best explored and completely mapped mine-induced fault zone to date, so it is of particular interest with regard to establishing relations between fault zone architecture and failure mechanics.

An essential theme of this study is the nature and mechanics of the formation of a quasiplanar fracture zone. Although the developnent of tensile cracks has proven amenable to mathematical analysis, the formation of planar

shear cracks has been largely ignored by fracture mechanicians. A major difficulty is that a shear crack cannot grow in its own plane, but rather extends out of its plane as a tensile crack, finally stabilizing with the crack oriented in the direction of the maximum principal compressive-stress σ_1 (e.g. Brace and Bombolakis, 1963; Sih, 1973). Some apparent exceptions to this generalization were reported by Holzhausen (1978) who managed to cause cracks in a rock-like material oriented at angles of 22½° or less to σ_1 to extend in their own plane. These experimental results will be discussed later.

Because of the difficulty of getting shear cracks to extend in their own plane, it seems likely that fault formation is not the result of the dynamic propagation of such cracks. Laboratory results have indicated that shear fractures in samples in triaxial compression somehow result from the coalescence of tiny microcracks oriented subparallel to σ_1, which develop as the axial stress approaches its maximum value. Laboratory experiments (Scholz, 1968; Peng and Johnson, 1972; Hallbauer et al., 1973; Lockner and Byerlee, 1979) have shown that microcracks form homogeneously throughout the sample at low levels of stress. As the state of stress approaches its ultimate level, an instability develops such that microcracks develop Preferentially within a band more or less coinciding with the eventual shear fracture. At present it is not clear what determines the orientation of the band of intense microcracks, but Rudnicki and Rice (1975) have analyzed the associated dilatancy in terms of elastic-plastic constitutive relationships and have predicted the developent of an instability in the form of a deformation band oriented roughly parallel to the direction of the maximum shear stress.

The incipient shear fractures form within these bands of intense subgrain-scale microcracking and much of the available evidence, including ours, suggests that this is the stage at which the intricate fault zone geometry is established. One of the primary intents of this report is to relate the observations of complex fault patterns to the factors responsible for the geometry of the incipient shear fractures. The underlying assumption here is that the only essential difference between the incipient faults and post-fracture faults involves the amount of shear displacement and the degree Of commination of rock within the fault zone.

OBSERVATIONS AND BACKGROUND

The fault zone under discussion occurred in the West Claims pillar in 1974 and was discovered where it cropped out in the south wall of a bay off the 49 level drive (tunnel) (Figure la). At that time, one of the more important issues regarding the mechanism of mine tremors was the extent of the corresponding faults. Did they have dimensions of tens of meters, as the underground evidence up to that time had suggested, or were they several hundred meters in extent as inferred from measurements of seismic source parameters (Spottiswoode and McGarr, 1975)? The network of inclined tunnels developed over the following 16 months revealed a great deal of unexpected complexity in the fracture zone and dimensions of at least 30 m, but the question of the overall extent was not answered. It did not prove possible to extend the tunnels far enough to encompass the entire fracture system.

A detailed structural mapping from the inclined tunnels indicated that the fault system consists of two quasi-planar shear zones, termed zones A and B (Gay and Ortlepp, 1979) and Ortlepp (1978) showed that the two zones correlate with seismic events that caused damage in September 1970. Shear zone B was associated with one of two reported tremors (magnitudes of 1.7 or 3.4) on September 5 and 6 and zone A was more definitely correlated with an event of magnitude 2.1 on September 23 (see also McGarr et al., 1979). Ortlepp (1978) also demonstrated that the two zones are related to the mine geometry as shown in Figure 1a.

The gold in the Witwatersrand mines occurs in reefs which are typically of the order of 30 cm thick and form broad planar beds dipping southward. The country rock above (hangingwall) and below (footwall) the reef is quartzite with a strength in uniaxial compression of 2 to 4 kb (e.g. Jaeger and Cook, 1969; McGarr et al., 1975). The mining operation consists of excavating thin tabular stopes roughly 1¼ m thick centered about the gold bearing reef and then tramming the ore out through tunnels in the footwall such as the 49 level footwall drive shown in Figure 1a. Because the stresses in the rock abutting the stopes become exceedingly high, the rock inevitably fails and a large fraction of this failure in E.R.P.M. is accounted for by tremors, sane of which cause considerable underground damage (McGarr, 1976).

Figure 1a is a plan view showing the approximate traces of shear zones A and B in the plane of the reef relative to the mine face position in September 1970. Shear zone B strikes east-west, dips northward, and Ortlepp (1978) has related it to the northward advancing face about 30 m to the south. Shear zone A strikes NW, dips toward the NE, and was assumed due to the face advancing toward the NE (Figures 1a and 1b). Both of the shear zones are typical of burst fractures observed in the Witwatersrand gold mines in that they are normal faults with a sense of displacement such as to accomodate the movement of rock into the nearest stopes (McGarr, 1971a). For example, we have presumed that the convergence of the stope on the lower-left in Figure 1b was the primary cause of the elastic strain build-up that resulted in shear zone A. Another common feature of these mine-induced faults is their control by the mine geanetry rather than pre-existing geological faults and joints. This report emphasizes observations and analysis of shear zone A rather than B because zone A could be more definitively associated with a particular seismic event and also because it was explored over a greater depth range.

Following the initial discovery of zone A a network of inclined tunnels were developed starting from the north sidewall of the 49 drive adjacent to the fan chamber (Figure 1). The raise at first went northward and upward and then fanned out in five different directions to follow the various branches of the fractures upward toward the mining horizon (Gay and Ortlepp, 1979). The cross section view of shear zone A (Figure 1b) is actually an "artist's impression" of the structure of the fracture system rather than a faithful description of the geometry. Although the individual fractures were mapped in considerable detail it was not possible to project these fractures unambiguously onto a cross section because of difficulties in correlating individual fractures between different branches of the inclined tunnel System.

Typical shear displacements across the shear zones ranged from about 4 to 10 cm (e.g. McGarr et al, 1979) and the sense of displacement was always as indicated by the large arrows in Figure 1b. A large scale feature of possible

significance, shown schematically in Figure 1b, is the variation in width of zone A. Where we first discovered this fracture system, on the 49 level, it was 10 to 20 cm wide (e.g. Figure 6d of Gay and Ortlepp, 1979). Up the dip the width of the zone increased to several meters as seen, for example, in Figure 6c of Gay and Ortlepp (1979).

State of stress. The ambient state of stress in the absence of mining at the depth (about 2 km) of shear zones A and B in ERPM is approximately represented by a maximum principal stress oriented in a near-vertical direction and having a magnitude of 530 bars with the other two principal stresses oriented more or less horizontally and having magnitudes of 265 bars, half of the overburden value (Gay, 1975; McCarr and Gay, 1978; McCarr et al., 1979). The ambient state of stress interacts with the mining to add a substantial amount of induced stress to the rock in the environs of the shear zones. The mine geometry near the shear zones (Figure 1) is quite complex so it is difficult to compute even an approximate stress field for this region, especially if one were to take into account the inelastic deformation (e.g. McGarr, 1971b).

To obtain some idea of the stress field near shear zones A, a simple two-dimensional calculation was performed using the method of Muskelishvili (1953) (e.g. Cook, 1963). We assumed that stress of magnitude 1 acted normal to the plane of the nearest mine excavation, modelled as a thin crack, to the south and southwest of shear zone A to produce an induced stress field. We also assumed that the stress acting parallel to the plane of the excavation was half of the component normal to the stope. The results of the calculation at selected points near shear zone A, as seen in cross section (Figure 1b), are indicated by number pairs. The numbers indicate the maximum and minimum principal stresses, respectively, in units of the stress acting perpendicular to the stope. If the mine face to the SW of shear zone A was the only factor altering the stress field then the unit of stress in Figure 1b would be about 540 bars, which is the overburden stress. In fact, the shear zones are within the isolated West Claims pillar and, in particular, the mining to the east, which was completed in 1948, induced large stresses in the area. Several approximate methods of stress calculation were used in an attempt to include the effects of the stope in the upper right of Figure 1b. The results indicate that the unit of stress might be as high as 1 kb at this writing. However, the results of the different methods show quite a lack of agreement and so we can only place broad limits of 540 bars to 1 kb on the stress unit in Figure 1b.

One of the interesting features of the stress field indicated in Figure 1b is the increase in the minimum principal stress in the up-dip direction. From the 49 level up to the level of mining the minimum stress increases by more than a factor of two. Note that the relative increase of σ_3 does not depend on our knowledge of the absolute level of the stress field and so this effect is reasonably independent of the various assumptions in the analysis.

En echelon offsets. As seen schematically in Figure 1b, the mine-induced shear zones consist of an echelon pattern of fractures occurring on a variety of scales. One of the most intriguing observations is that the sense of offset is always opposite to the sense of displacement. That is, for right lateral displacement as viewed in cross section, the trace of the fracture

steps to the left as illustrated in Figure 2a; similarly, for left lateral displacement the offsets are to the right. The end points of the main fractures are connected by a series of secondary shear fractures, which in some cases offset the primary fractures by small displacements but do not extend beyond them. The *en* echelon pattern occurs over a range of length scales from less than a centimeter to more than a meter in the shear zone under discussion.

The line drawing of Figure 2b highlights a number of smaller en echelon patterns within the large offset and also illustrates the nature of the shear displacement across this region. The pre-existing joint, labeled J, has been displaced 2-3 an across each of the primary shear fractures with little obvious deformation in the region between the offset ends. It appears that the segment of joint within the zone of overlap may have experienced a slight clockwise rotation as viewed in Figure 2b. It is also of interest to note that the joint appears to have undergone much less shear displacement than the near-parallel secondary fractures; that is, comminution of the quartzite in the joint is much less evident than for the secondary fractures.

The secondary fractures within the large offset region in Figure 2b appear to be structurally controlled by the primary shear fractures. We see that many of the secondary fractures seem to originate from the end regions of fracture segments composing the primary shear faults. Furthermore, as mentioned previously, the secondary fractures do not extend beyond the overlapping primary fractures. Another manifestation of the scale-independence of the fracture pattern is the relationship between the spacing of the secondary fractures and the amount of offset of the primary fractures. In Figure 2 the secondary fractures connecting the primary shears are 22 to 25 cm long and separated by about 4 to 8 cm and those between the small offset fractures just to the left of the center of Figure 2a have lengths of about 4 an and spacings of roughly 1 an. Generally, then, the ratio of length to spacing of the secondary fractures *is* approximately 4. These observations all indicate that the secondary fractures, as their name suggests, are generated as a result of the primary shear fractures.

On the average, the ratio of overlap b to offset a, as defined in Figure 3, is approximately 4 but there is considerable variation about this mean, 20 measurements of a and b from photographs of en echelon offsets within the shear zones yielded ratios b/a ranging from 1.3 to 6.6. The arithmetic average is 4.1 and the geometric mean is 3.7; for each type of mean the standard deviation is 1.6. In any case, b/a does not show any systematic variation with dimension.

Part of the exposure of shear zone A where it was first discovered in the south sidewall of the fan chamber (Figure la) was previously interpreted by Gay and Ortlepp (1979, Figure 6d) and McGarr et al. (1979, Figure 5) as a bifurcating-and-coalescing fracture. On closer inspection, however, this turned out to be another en echelon pattern with an unusually large value of b/a. In fact, it seems that there are no bifurcations in the individual fractures along the dip (parallel to the shear displacement) of shear zone A. Along strike, however, the fractures are observed to bifurcate and coalesce. Thus, the amount of offset, a, seen in Figure 3 would presumably show some variation along the direction perpendicular to the figure.

The shape of any of the individual shear fractures forming the fracture zones is fairly consistent as seen, in Figure 2 and idealized in Figure 3. Each fracture has a linear portion subparallel to the dip of the overall zone and the end regions, termed "feather fractures," tend to curve into the vertical direction. The sigmoidal (or mirror-image sigmoidal) units on a variety of scales are nested together in en echelon patterns to form the fracture zone.

Microscopic observations. Gay and Ortlepp (1979, Figure 9) performed microscopic analyses of thin sections of wall rock adjacent to the shear fractures and found evidence for a pervasive distribution of intragranular microfractures oriented subparallel to the maximum principal stress. Away from the major shear fractures the distribution of microcracks was considerably subdued. Distortion of the microcrack by shear fractures tended to confirm the belief that the formation of the microcracks preceded the shear displacement.

In addition to the microfractures Gay and Ortlepp (1979) reported two sets of larger scale fractures in the wall rock within an en echelon offset. One set appeared to be shear fractures showing small displacments of the order of 0.2 mm oriented in the conjugate direction ($\sim 60°$) to the primary shear direction. The other set consists of fractures oriented approximately Parallel to the microfractures and are interpreted as extension cracks as they show no shear displacement.

DISCUSSION

We now make a brief case for a high degree of similarity between the fractures observed underground and in laboratory samples. Then we consider a particularly relevant set of experiments that bear on the initial development of shear fracture planes and then use these laboratory results as a point of departure for analyzing the underground fracture patterns in terms of the stress field induced by an isolated crack and by interactions between cracks.

The important similarities between the fractures observed underground and those in laboratory samples are as follows. (1) The development of intragranular microcracks oriented subparallel to the direction of the maximum Principal stress precedes the shear failure. In both cases the microcracks are most pervasive near the planes of shear displacement. (Hallbauer et al., 1973; Peng and Johnson, 1972; Scholz, 1968; Lockner and Byerlee, 1979; Gay and Ortlepp, 1979). (2) The fracture patterns in the laboratory samples in triaxial compression also form en echelon patterns consistent in sense with those observed underground. On the scale of a laboratory sample the en echelon offsets are normally seen as steps on one fracture surface opposing the motion of the other surface (e.g. Paterson, 1958). (3) The fault gouge shows a similar degree of comminution in both cases (Spottiswoode, 1979).

Accepting for now the similarity between failure in the lab and in the mine, we now consider some experiments on ERPM footwall quartzite by Hallbauer et al. (1973). These authors tested a suite of cylindrical samples in a stiff machine to various points on the stress-strain curve; typical levels of confining stress near the peak of the loading curve were about 300 bars. By studying thin sections of the various samples under the microscope they were

able to establish that most of the microcracks are intragranular, near-parallel to the axial direction and form at levels between about 80% and 100% of the peak stress. From their photomicrographs it appears that somewhat before peak stress an incipient shear plane forms by means of linking up of microcracks. Kranz (1979) has recently presented sane electron micrographs showing in detail some mechanisms for crack coalescence. No major shear displacement occurs, however, until the stress-strain curve is significantly past its peak.

There are several important results from the study of Hallbauer et al. in the present context. First, the formation of the shear fracture is primarily a tensile process. No dynamic shear fracture propagation is involved. Second, at the time of formation of the incipient shear fracture the specimen is still in a strain-hardening portion of the loading curve. Third, the geanetry of the fracture is largely established before any substantial strain softening occurs. These findings are assumed here to apply also to the developent of the fractures composing the mine-induced shear zones.

On the basis of the laboratory results we assume that at some point during the build up of stress in the rock the intragranular microcracks coalesce to form a larger scale crack whose plane is oriented at about 30° to the direction of the maximum principal stress, σ_1. Once this crack develops we can analyze it as a shear crack, because of its orientation. Under the influence of the applied stress field this incipient shear crack deforms and generates induced stresses which influence the developent of successive fractures. This is the point at which we begin our analyses of interactions between shear cracks under the influence of a broad scale stress field in order to gain sane insight into factors responsible for the observed fracture patterns.

The following analyses assume a two-dimensional plane strain model and the solutions for stress and deformation are obtained using a method of successive approximation described by Pollard and Holzhausen (1979) and Segall and Pollard (1978). Each crack is assumed to have a frictional resistance to shear displacement proportional to the normal stress, σ_n, acting on the plane of the fracture. The assumed dimensions in the following examples are arbitrary and were chosen to illustrate the particular geometry of Figure 2. The following analysis is divided into three successive stages of fracture developent starting with the case of a single crack in an applied stress field.

In Figure 4 we illustrate the tendency of a 4 m long crack to induce failure in the adjacent rock. The primary fracture extends from $x = -2$ m to $x = +2$ m, but only the right-hand half of the crack is shown because the picture is antisymmetric about the plane $x = 0$. The assumed ambient state of stress is indicated in the lower right-hand corner and was originally intended to be similar to the typical state of stress in the environs of shear zones A and B. In fact, it seems that the assumed minimum principal stress is too low (Figure 1b), but until more exact estimates of the state of stress near shear zone A become available we have elected not to repeat the analysis. We note that if the ratios σ_3/σ_1 are as high as suggested in Figure 1b, then shear displacements across pre-existing cracks or in intact rock are difficult to explain in terms of laboratory rock mechanics results.

With an assumed coefficient of friction $\mu = 0.7$ the crack in Figure 4 has a maximum shear displacement of about 2.2 mm, which is much less than the typical observed displacements of 4 to 10 cm (McGarr et al.. 1979) because we are considering an isolated crack. As will be seen, the large shear displacements can only occur after a long series of shear cracks interact inelastically.

As the crack deforms under the influence of the applied stress field it induces new stresses which, in turn, will affect the developent of additional fractures. The relationship between the total stress field (applied and induced) and the tendency for new fractures to form is not entirely clear and so we have to rely on laboratory observations. Shear failure in rocks under compression is normally observed to occur according to the Mohr–Coulomb failure criterion (e.g. Jaeger and Cook, 1969)

$$|\tau| - \mu\sigma_n = S_o$$

where S_o is a material constant, and τ is the shear stress acting on a plane oriented in the optimum direction for failure, taken here as 300 to the direction of σ_1. On this basis the function we have chosen as a measure of the tendency of the stress field to cause failure is $F = |\tau| - 0.7\ \sigma_n$. If, $\sigma_3 < 0$ at a particular point where F has a high value, then we assume the formation of a tensile fracture oriented parallel to σ_1, rather than a shear fracture. Generally, values of F that are high compared to the ambient level of 263 bars are considered to indicate likelihood of further failure.

Spacing of parallel fractures. From the contours of F in Figure 4 it is clear that if a fracture were to form parallel to the original crack and between $x = -2$ and $+2$ m the new crack would lie at least 1 to $1\frac{1}{2}$ m above or below the $y = 0$ plane; otherwise fracture formation in a region of low F would be implied. Generalizing on this point, we expect parallel shear fractures to be separated by a distance of 1/11 to 1/3 of the fracture dimensions in stress regimes similar to that considered here. Thus, the fairly consistent crack spacings noted for the secondary fractures in Figure 2 are expected on the basis of the analysis of an isolated crack (Figure 4).

New fractures. The high values of F contoured in Figure 4 form two lobes, one extending downward and slightly leftward from the fracture tip and the other extending ahead and somewhat upward fran the tip. New fractures have been sketched into the high–F regions subject to various constraints. Immediately ahead of and below the crack tip at $x = +2$ m $\sigma_3 < 0$ and so tensile cracks oriented parallel to the local direction of σ_1 are indicated in this portion of Figure 4. This result simply confirms the tendancy of shear cracks to stabilize rather than propagate in their own planes (e.g. Brace and Bombolakis, 1963). The extension cracks calculated to form in the close vicinity of the fracture tip (Figure 4) seem to match closely the observed "feather fractures" which extend out of the planes of the en echelon fractures in Figure 2. Those extension cracks are confirmed to lengths of less than 20 cm by the induced stress field. Longer cracks would experience compressive stress across their distal ends.

In the high-F region away from the fracture tip σ_3 is positive and so we expect shear failure in one of two conjugate directions at 300 to the local direction of σ_1. The secondary shear fractures sketched in Figure 4 have been drawn in one of the two possible directions such as to allow the maximum length of shear fracture within the high-F zone.

The high-F lobe extending ahead of the primary fracture is particularly interesting because this is where shear fractures are expected to form that will eventually interact strongly with other fractures in the same approximate plane. First, we notice that this lobe is centered slightly above the plane of the initial crack and so we expect new shear fractures within this zone to mostly lie above the $y = 0$ plane. The new shear crack shown in Figure 4 was arbitrarily assumed to be about 10 cm above the initial crack. We see that the new shear crack is not predicted to overlap with the original crack on the basis of this single fracture analysis.

The analysis illustrated in Figure 4 indicates that there will be a tendancy for new shear fractures to be offset from the initial fractures in the same sense as in Figure 2, but allows for the possibility of the other sense of offset. If a shear fracture formed in the $y < 0$ region of the high-F lobe it would almost certainly propagate into the tip of the original crack (Segall and Pollard, 1978) and so it would not be distinguishable as a separate offset fracture.

The analysis illustrated in Figure 5 Includes two primary shear cracks parallel to the x axis and offset by 30 cm as anticipated on the basis of observations in the mine. The single crack shown in Figure 4 does not induce a stress field that would lead to formation of another parallel primary crack of comparable length. We speculate that this second primary shear crack formed in response to stresses induced by a much more extensive zone of shear parallel to the two cracks but not visible in this cross section. The geometry of the two primary shear cracks is consistent with the induced stress field of Figure 4. That is, the second crack lies in a region of relatively great F and does not extend into the low-F region.

Tensile cracks leading away from the end of the primary shear cracks in Figure 5 have lengths such that these fractures are in equilibrium with the local stress field. That is, if the tensile crack initiates in the zone of large negative values of σ_3 near the tip of a primary shear and propagates away from the end region, then the mode I stress-intensity factor, K_I, initially has a large positive value indicating a marked propensity for further propagation. As the crack lengthens K_I diminishes and finally becomes negative at about the crack length of 10 an shown in Figure 5. Interestingly, a comparison of the stress field shown in Figure 5 with that calculated for a similar case but without the two tensile cracks, showed that these "feather fractures" have very little effect on the induced stress field.

As before, there is a region of negative σ_3 immediately ahead of and below each of the tips of the primary shear fractures where we anticipate further tensile failure, as indicated schematically in Figure 5. Of primary interest, however, are the high-F regions extending ahead of each of the primary shears. On the basis of the induced stresses calculated in these zones shear fractures are predicted to form at distances of up to roughly 40 an ahead of each primary fracture tip, as indicated shematically in Figure 5. **It should be reemphasized that the illustrated fractures in the high-F regions**

were sketched somewhat arbitrarily and only represent one of many possibilities. Nevertheless, it is clear that the results of the analysis illustrated in Figure 5 predict amounts of overlap by the formation of shear cracks ahead of the initial shear fractions that are entirely consistent with the observations (e.g. Figure 2).

As illustrated in Figure 6 we have taken the analysis to the third stage and calculated the stress field induced by offset primary shear cracks that overlap by 20 cm. This analysis assumes that the primary shear fractures in Figure 5 have been extended by 10 cm because of strong interactions between them and the new shear fractures immediately ahead of their tips. Tensile cracks were not explicitly included in the analysis of this case. As mentioned before this fracture configuration is intended to be similar to that shown in Figure 2.

Contours of F show the two high-value lobes extending from each fracture tip region, as was seen in the two previous examples, but, of greater interest is the marked high-F region between the offset ends of the primary fractures. As before, shear fractures having the orientation allowing the longest fractures have been added and we see that these predicted secondary fractures coincide quite nicely with those observed in Figure 2 although the actual fractures may be rotated clockwise slightly relative to the calculated planes of failure.

Interestingly, the elastic interaction between the offset fractures in Figure 6 has very little effect on the peak shear displacements even though it clearly has a major effect on the state of stress between the two cracks. The peak displacements across the fractures of Figure 6 are 2.9 mu whereas the peak displacements for the isolated 4 m fracture is 2.2 mu. Presumably, the strong interactions between fractures resulting in shear displacements of 6 cm or so require inelastic deformation of the material between adjacent primary shear cracks. The conjugate shear fractures shown in the middle of Figure 6 must eventually serve as an important mechanical link between the offset cracks during the major stress drop.

CONCLUSIONS

Exploration of shear zones A and B revealed considerable unexpected complexity, but there is nevertheless some system to the fracture patterns. Because these fractures only failed once, it was possible to relate the post-failure observations to the pre-failure regime when we presume the incipient shear fractures were developing. It seems likely that the systematic features, highlighted in Figure 3 for instance, are much more apparent in the mine-induced fractures than in natural fault zones that have experienced repeated failure.

The shear zones consist of a complex series of fracture segments of various lengths from about 1 cm up to 4 or 5 m. The various segments, however, were in fact made up of many nested shorter segments (e.g. Figure 2). One of the most interesting features of the shear zones is the similarity of their geometries over a wide range of scales. Individual fractures appeared to be oriented at roughly 30° to the local direction of σ_1 (e.g. Gay and Ortlepp, 1979) whereas the en echelon offsets were such as to make the overall shear zone more parallel to the direction of τ_{max}, the maximum shear stress.

Probably the most important assumption in our analysis of fracture development is the assertion that the fracture geometries are established before large scale strain softening of the shear zone commences. This assumption relies heavily on the experimental results of Hallbauer et al. (1973) but it should be noted that all of the observations of shear zones A and B (Gay and Ortlepp, 1979) are consistent with the stable development of the crack patterns. That is, the fracturing is highly ordered on scales ranging from less than a grain dimension up to 5 m or more. Furthermore, a cataclysmic event might be expected to produce considerable grain boundary rupturing, which was not observed (Gay and Ortlepp, 1979). If our underlying assumption is correct then the actual seismic event, corresponding to the major stress drop, simply involves substantial increases in shear displacement across fractures whose geanetries are already established. The most important effect associated with the large displacements is the generation of fault gouge (Spottiswoode, 1979).

By analyzing the interaction between a single crack and the ambient stress field we confirmed the results of previous studies to the effect that a shear crack could not extend in its *own* plane but rather terminates in an extension crack that stabilizes more or less in the direction of σ_1. Further failure occurs by means of subparallel en echelon cracks as indicated in Figure 4. This seems to be a viable mechanism for the extension of shear failure in nearly the same plane as an initial crack. This also appears to be the mechanism by which shear cracks studied by Holzhausen (1978) extended "in plane". As the applied deviatoric stress was increased in these experiments the initial crack, oriented at 22½° to σ_1, extended at first out of plane by means of a short fracture approximately parallel to σ_1. Further increase of stress resulted in a series of offset fracture segments subparallel to the initial crack and showing shear displacement. All of the observed offsets were to the right for left-lateral shear displacement.

Before an incipient shear crack forms the rock has deformed inelastically by means of microcracks oriented subparallel to σ_1 and various studies have shown that somewhat before the ultimate stress is reached these subgrain sized cracks preferentially form in bands along the eventual shear faults. So far, it is not known exactly why these dilatant deformation bands tend to be more or less parallel to τ_{max} or what determines their thickness. Both in the laboratory studies and possibly in shear zone A there is an indication that a higher confining stress leads to broader zones of shear failure (e.g. Tullis and Yund, 1977). In the case of shear zone A we noted in Figure 1b the qualitative correlation between increasing width of shear deformation and increasing σ_3 in the up-dip direction along the fracture zone fran the 49 level where it was first discovered. The primary conclusion of this study is that the consistent features of the shear zone geanetry can be predicted to a large extent on the basis of elastic interactions involving multiple cracks and an applied stress field. These consistent elements of the shear zone architecture (Figure 3) include: (1) fracture offsets of the opposite sense to that of the shear displacements with ratios of overlap to offset averaging roughly 4; (2) tensile or "feather" fractures, oriented subparallel to the direction of σ_1, terminating the shear fracture segments; (3) secondary shear fractures connecting the overlapping primary shears with an orientation appropriate for shear failure conjugate to that of the primary fracture.

The elatic analysis utilized here probably cannot be used to analyze the development of the fracture system after the offset fracture segments begin to interact strongly. We speculate that after the geometry illustrated in Figure 6 is established either a further increase of stress or a weakening of the zone of secondary fractures occurs such that the offset no longer serves as an effective barrier to shear displacement. The observations suggest that the large shear displacements, of the order of centimeters in shear zone A, are accanodated within the overlapping region by the rotation of blocks defined by the secondary shear fractures. For example, in Figure 2b the joint seems to have rotated clockwise slightly. For 6 cm of total shear displacement across this region we expect roughly 150 to 200 of block rotation, if the shear displacement is accommodated in this way. Note that the shear displacement across the secondary fractures that is associated with block rotation is opposite in sense to the conjugate shear failure that appears to have originally generated these faults (Figure 6).

After an en echelon offset ceases to be a "barrier" the two cracks effectively become one longer crack with correspondingly greater equilibrium shear displacements. This process is unstable because strain energy is released and the level of induced stress on adjacent offsets is correspondingly increased, possibly leading to further shear displacement.

ACKNOWLEDGMENTS

We thank Rand Mines Ltd. and the Chamber of Mines of South Africa for providing financial support for this project. Extensive discussions with Paul Segall and Gary Holzhausen helped to clarify some of the issued discussed here.

REFERENCES

Brace, W. F. and E. B. Bombolakis, A note on brittle crack growth in compression, J. Geophys. Res., 68, 3709–3713, 1963.

Cook, N. G. W., The seismic location of rockbursts, Proc. Fifth Rock Mechanics symposium, Pergamon Press, Oxford, 493–516, 1963.

Gay, N. C., In situ stress measurements in Southern Africa, Tectonophysics, 29, 447-459, 1975.

Gay, N. C. and W. D. Ortlepp, The anatomy of a mining–induced fault zone, Bull. Geol. Soc. Am., in press, 1979.

Hallbauer, D. K., H. Wagner and N. G. W. Cook, Some observations concerning the microscopic and mechanical behaviour of quartzite specimens in stiff, triaxial compression tests, Int. J. Rock Mech. Min. Sci. and Geomech. Abstr., 10, 713–726, 1973.

Holzhausen, G. R., On the propagation of fractures inclined to the direction of uniaxial compressive stress in a rook–like material, Westerly granite, and plexiglass, Internal Report 54102–1, Norges Geotekniske Institutt, Oslo, Norway, 1978.

Jaeger, J. C. and N. G. W. Cook, Fundamentals of Rock Mechanics, Methuen, London, 1969.

Kranz, R. L., Crack–crack and crack–pore interactions in stressed granite, Int. J. Rock Mech. Min. Sci. and Geomech. Abstr., 16, 37–47, 1979.

Lockner, D. and J. Byerlee, Development of fracture planes during creep in granite, Proc. 2nd. Conference on Acoustic Emission, Rock Mechanics Dept. of Pennsylvania State University, Trans. Tech. Publications, Clausthal, Germany, in press, 1979.

McGarr, A., Violent deformation of rock near deep-level, tabular excavations - seismic events, Bull. Seism. Soc. Am., 61, 1453-1466, 1971a.

McGarr, A., Stable deformation of rock near deep-level tabular excavations, J. Geophys. Res., 76, 7088-8106, 1971b.

McGarr, A., Seismic moments and volume changes, J. Geophys. Res., 81, 1487-1494, 1976.

McGarr, A., S. M. Spottiswoode and N. C. Gay, Relationship of mine tremors to induced stresses and to rock properties in the focal-region, Bull. Seism. Soc. Am., 65, 981-993, 1975.

McGarr A. and N. C. Gay, State of stress in the earth's crust, Ann. Rev. Earth Planet. Sci., 6, 405-436, 1978.

McGarr, A., S. M. Spottiswoode, N. C. Gay and W. D. Ortlepp, Observatons relevant to seismic driving stress, stress drop, and efficiency, J. Geophys. Res., 84, in press, 1979.

Muskhelishvili, N. I., Some Basic Problems of the Mathematical Theory of Elasticity, Noordhoff, Groningen, 1953.

Ortlepp, W. D., The mechanism of a rockburst, Proc. 19th U.S. Rock Mech. Symp., Stateline, Nevada, 476-483, 1978.

Paterson, M. S., Experimental deformation and faulting in Wombeyan marble, Bull. Geol. Soc. Am., 69, 465-476, 1958.

Peng, S. and A. M. Johnson, Crack growth and faulting in cylindrical specimens of Chelmsford granite, Int. J. Rock Mech. Min. Sci. and Geomech. Abstr., 9, 37-86, 1972.

Pollard, D. D. and G. Holzhausen, On the mechanical interaction between a fluid-filled fracture and the earth's surface, Tectonophysics, 53, 27-57, 1979.

Rudnicki, J. W. and J. R. Rice, Conditions for the localization of deformation in pressure-sensitive dilatant materials, J. Mech. & Phys. of Solids, 23, 371-394, 1975.

Scholz, C. H., Experimental study of the fracturing process in brittle rocks, J. Geophys. Res., 73, 1447-1454, 1968.

Segall, P. and D. Pollard, Two mechanisms for fault stability, EOS, Trans. Am. Geophys. Union, 59, 1205 (abstract), 1978.

Sih, G. C., Methods of Analysis and Solutions of Crack Problems, Noordhoff, Leyden, 517 pp., 1973.

Spottiswoode, S. M., Fault gouge, driving stress and seismic efficiency, submitted to J. Geophys. Res., 1979.

Spottiswoode, S. M. and A. McGarr, Source parameters of tremors in a deep-level gold mine, Bull. Seism. Soc. Am., 65, 93-112, 1975.

Tullis, J. and R. A Yund, Experimental deformation of dry Westerly granite, J. Geophys. Res., **82**, 5705-5718, 1977.

FIGURE CAPTIONS

Figure 1a A plan view of the mine geanetry in the southern portion of the West Claims pillar. The approximate traces of shear zones A and B on the plane of mining are shown. The 49 level footwall drive is about 25 to 30 m below the mine stope.

Figure 1b Cross section view along A–A' showing the relationship of shear zone A to the mining. The indicated fracture pattern within zone A is schematic and not intended to be exact. Shear zone B has not been included. The number pairs beside the dots indicate estimated levels of maximum and minimum principal stresses.

Figure 2a Photograph of shear zone A as it crops out on the north sidewall of the 49 level drive.

Figure 2b Line drawing illustrating the fracture geometry of Figure 2a. The most prominent pre–existing joint is labeled J.

Figure 3 Schematic diagram of fundamental fracture pattern observed in the mine–induced fault zones and their probable relationship to the broad scale state of stress.

Figure 4 The stress field of an isolated shear crack, extending from x = –2 m to x = +2 m, and the ambient stress field indicated in the lower right. The contours are of the function $F = |\tau| - 0.7\ \sigma_n$ with the ambient level of F being 262 bars. Fractures, indicated by thin lines, have been sketched somewhat arbitrarily into areas of high F where the induced stresses are expected to generate further failure. The inset shows more details of the tensile zone near the crack tip which is outlined by a dashed contour.

Figure 5 The effect on the stress field of interactions involving two 4 m shear cracks offset by 20 cm and tensile fractures extending from their end regions. The contours are as described in Figure 4. Additional fractures have been sketched in as thin lines in the regions of particularly high values of F. As in Figure 4 the tensile zone is bounded by a dashed contour.

Figure 6 Values of F in the region about the overlapping end regions of two 4 m shear cracks under the influence of the ambient stress field shown in the lower right–hand portion of the figure. In regions where F is high, secondary failure is anticipated. Of particular interest are the secondary shear cracks between the two primary cracks.

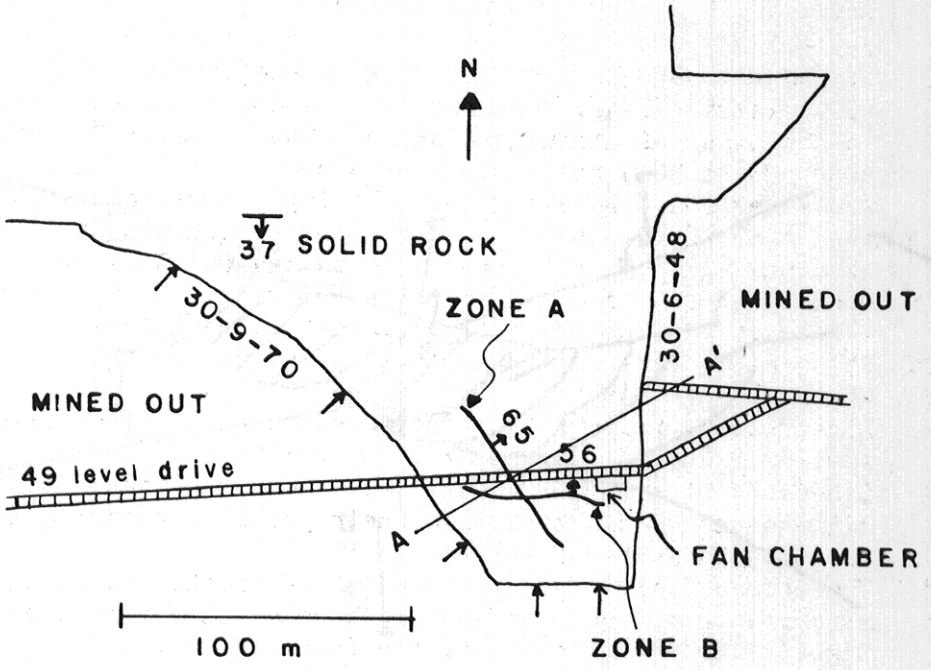

Figure 1a

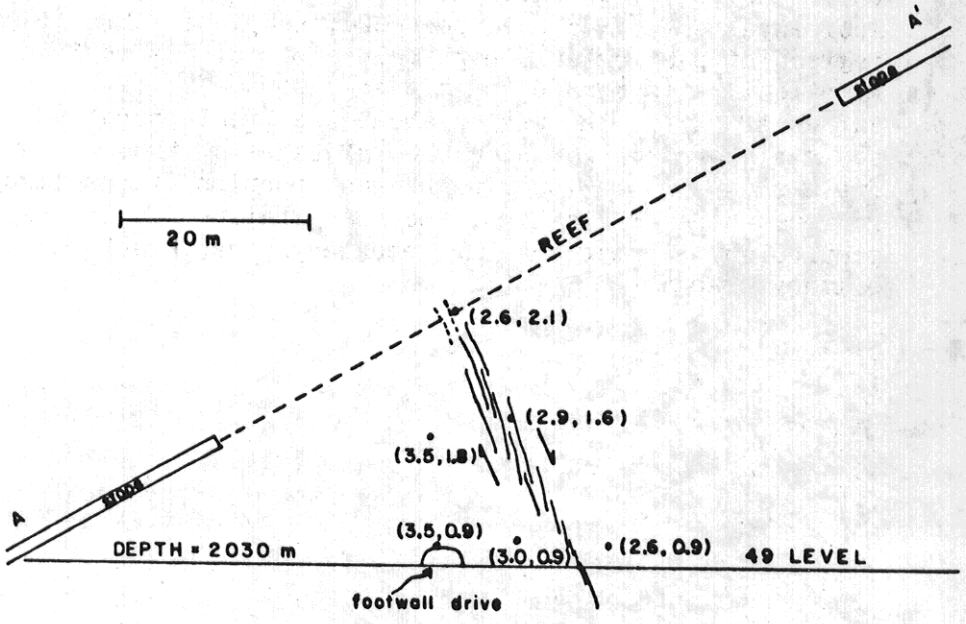

Figure 1b

Figure 2a

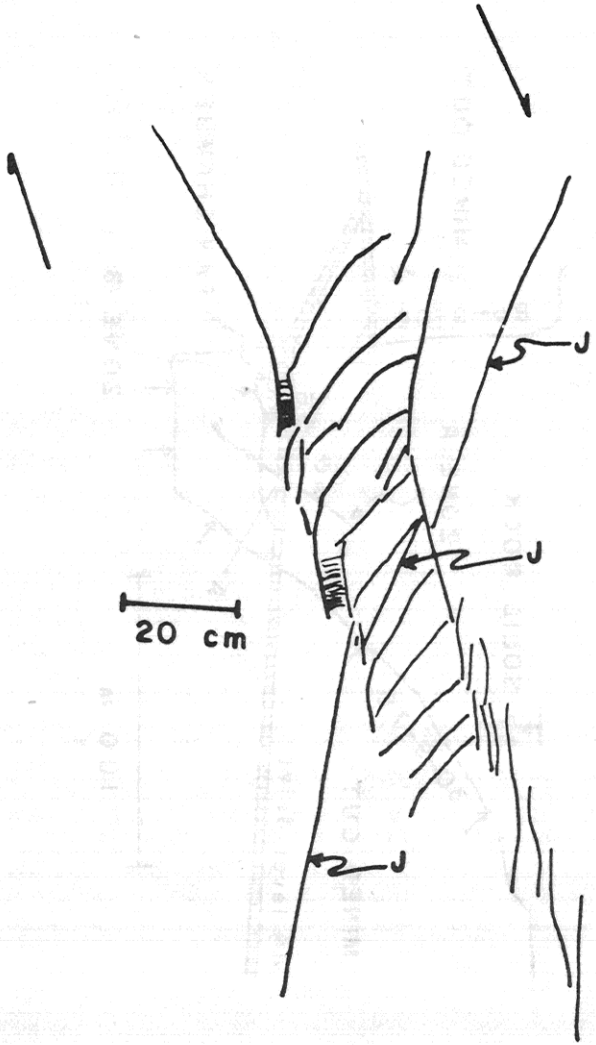

Figure 2b

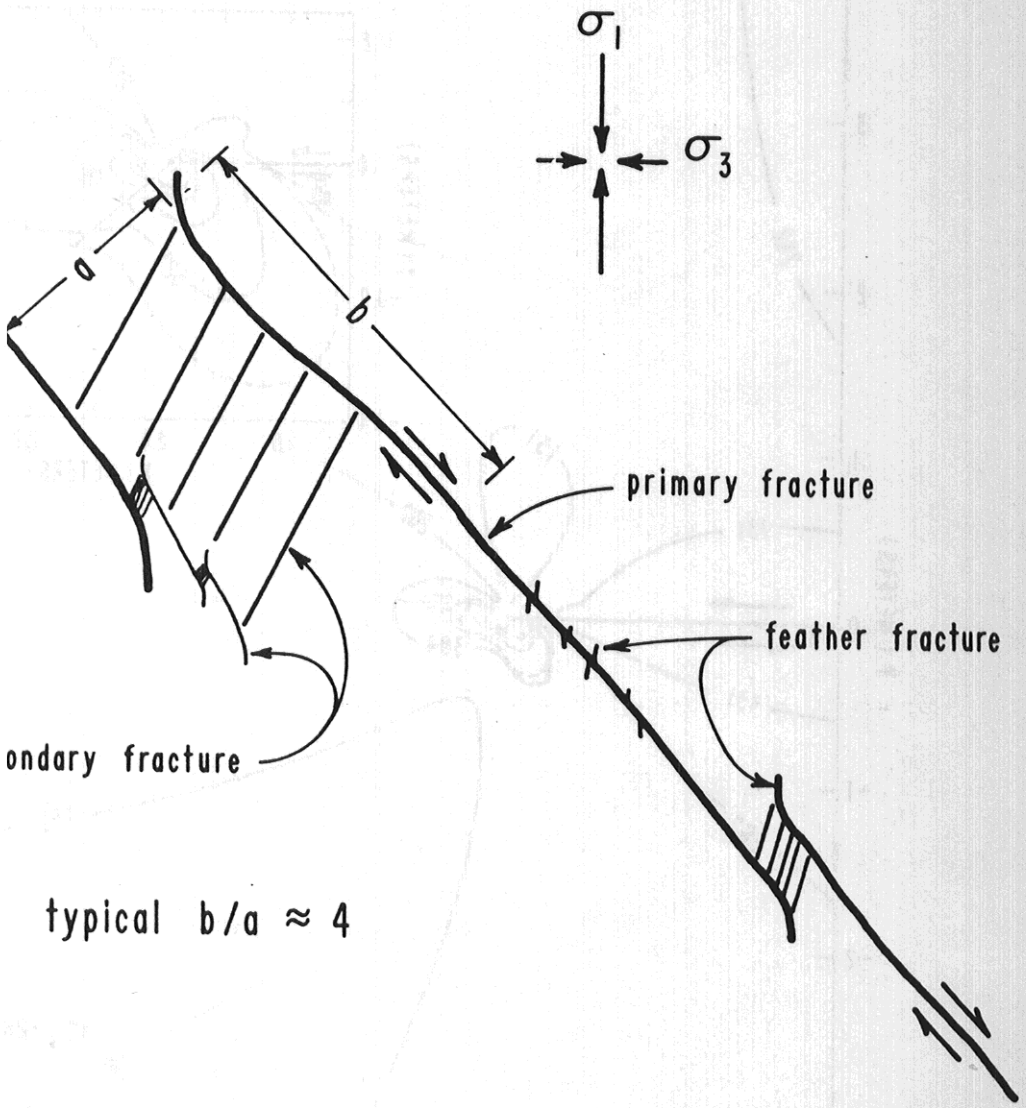
σ1
σ3
a
b
primary fracture
feather fracture
ondary fracture
typical b/a ≈ 4

Figure 3

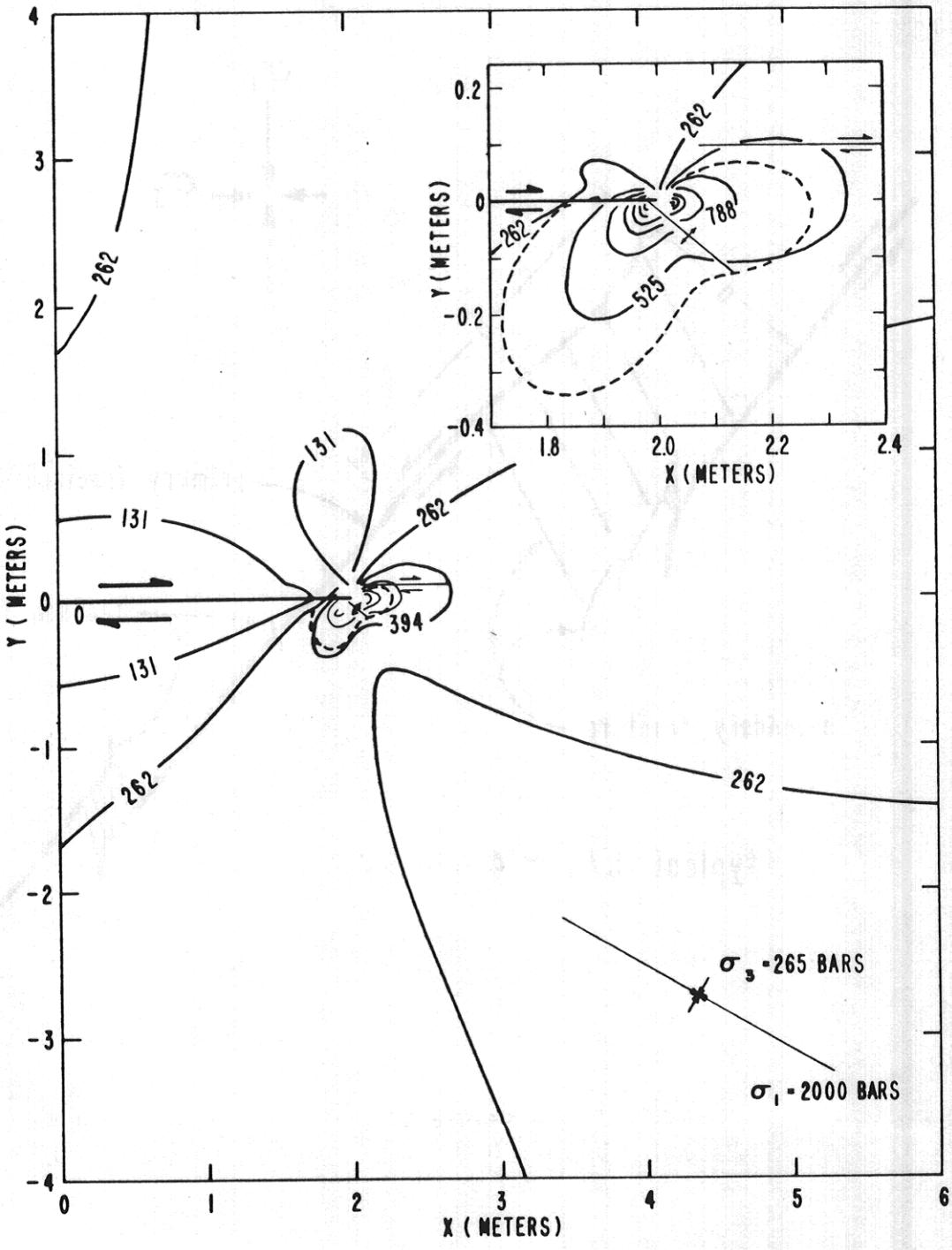
262
131
131
262
0
131
394
262
262
σ_3 = 265 BARS
σ_1 = 2000 BARS
Y (METERS)
X (METERS)
0.2
0
-0.2
-0.4
1.8
2.0
2.2
2.4
262
788
262
525

Figure 4

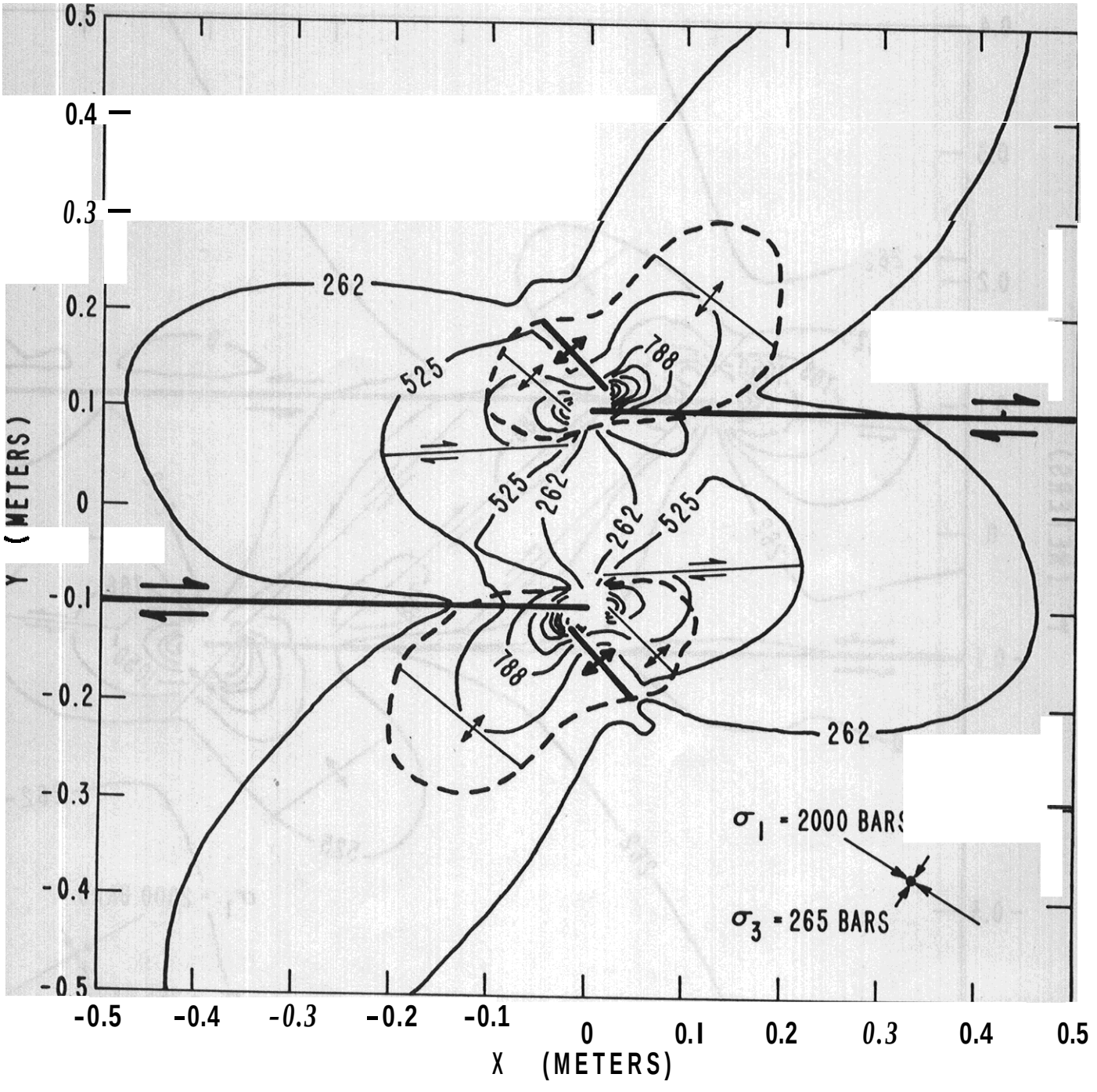
0.5
0.4
0.3
0.2
0.1
0
-0.1
-0.2
-0.3
-0.4
-0.5
Y (METERS)
-0.5
-0.4
-0.3
-0.2
-0.1
0
0.1
0.2
0.3
0.4
0.5
X (METERS)
262
525
788
525
262
262
525
788
262
σ1 = 2000 BARS
σ3 = 265 BARS

Figure 5

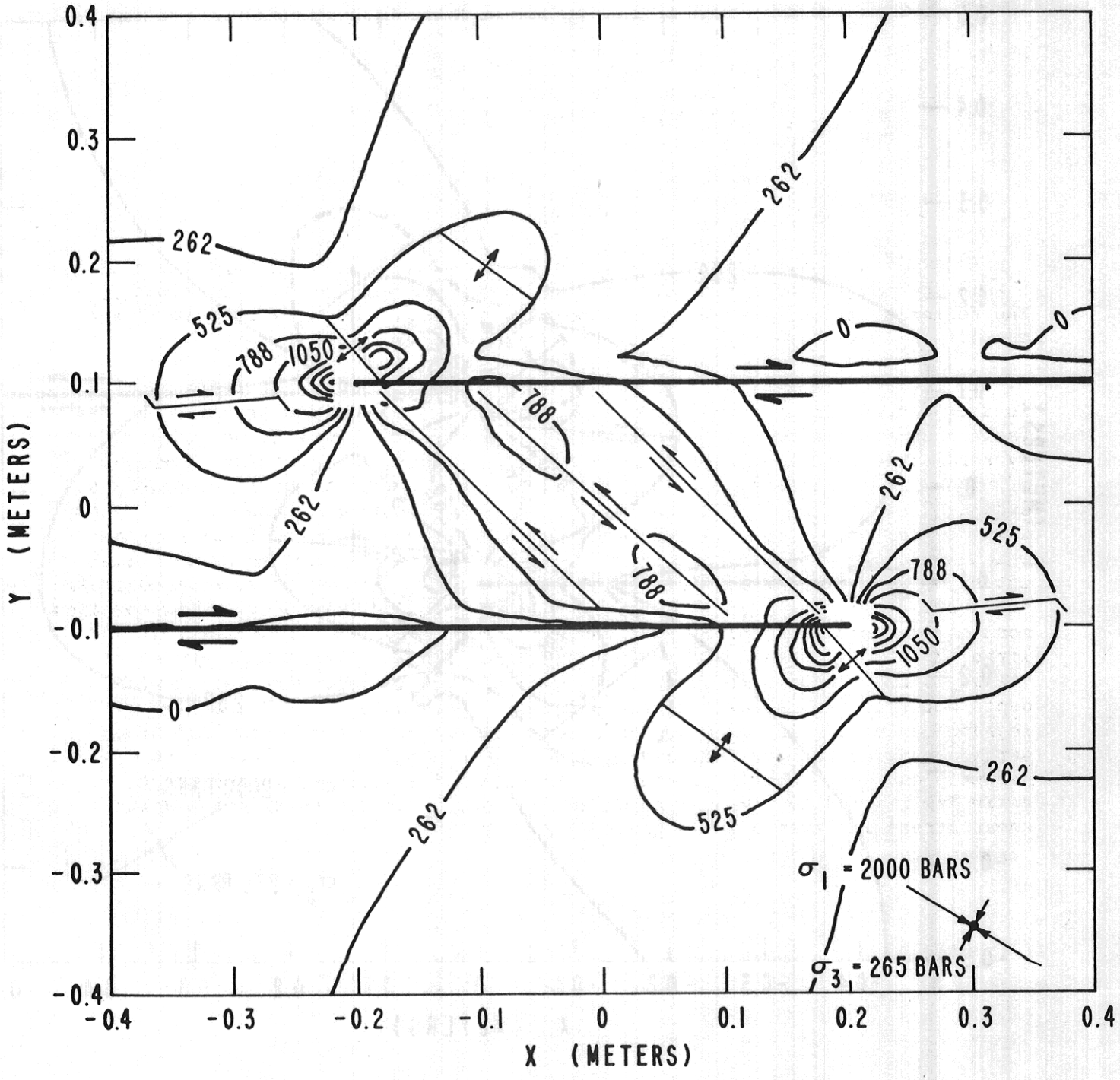
0.4
0.3
0.2
0.1
0
-0.1
-0.2
-0.3
-0.4
Y (METERS)
-0.4
-0.3
-0.2
-0.1
0
0.1
0.2
0.3
0.4
X (METERS)
262
525
788
1050
0
σ_1 = 2000 BARS
σ_3 = 265 BARS

Figure 6